Aalborg Universitet

AALBORG UNIVERSITY

DENMARK

Effect of Damage and Support Damping Mechanisms on Unimorph Piezoelectric Energy Harvester

Khazaee, Majid; Rezaniakolaei, Alireza; Rosendahl, Lasse

Document Version
Accepted author manuscript, peer reviewed version

Link to publication from Aalborg University

Effect of Damage and Support Damping Mechanisms on Unimorph Piezoelectric Energy Harvester

Majid Khazaee, Alireza Rezania[*], Lasse Rosendahl

Department of Energy Technology, Aalborg University, Pontoppidanstræde 111, 9220 Aalborg East, Denmark

1

2 **Abstract**

3 Damping plays a critical role in power generation by piezoelectric energy harvesting (PEH), and yet there

4 is the lack of sensitivity studies on different sources of damping. In this paper, two damping sources in

5 unimorph PEH, namely support loss and damage damping mechanisms are experimentally investigated.

6 Variation of the power generation are evaluated with respect to the sources of damping. Accordingly, the

7 power generation model is developed according to the experimental results in this work and using a

8 single degree of freedom analytical model. This study has focus on debonding effect, as an internal

9 damping source, and support loss, as a critical source of external energy dissipation. The results show

10 that the debonding reduces the output power dramatically at resonance and, particularly, at anti-resonance

11 frequencies. Moreover, investigation of the support loss shows that material of clamp as well as

12 installation torque have an impact on the support loss and, consequently, affect the output power.

13 **Keywords:** Piezoelectric Energy Harvesting, Unimorph, Damping Effect, Debonding Effect, Support

14 Loss.

15

16 1. Introduction

17 With the recent development in electronics, e.g. the decrease in power consumption (Khaligh et al.,

18 2010), low power energy harvesting from thermal and kinetic sources of energy is being widely

---

[*] Corresponding author: Alireza Rezaniakolaei. E-mail: alr@et.aau.dk

1   considered as an essential tool to introduce self-powered devices for elaborating system abilities in terms

2   of life time and accessibility of remote systems (Ahmed et al., 2017). Furthermore, energy harvesting

3   systems can be manufactured using additive manufacturing techniques (Mortazavinatanzi et al., 2018)

4   for non-flat surfaces with flexible ink-based (Https://www.piezotech.eu, n.d.; Qing et al., 2018). Among

5   the energy harvesting mechanisms, piezoelectric energy harvesters (PEHs) have drawn much attention

6   due to structure simplicity and ease of integration into the host structure (Khazaee et al., 2019).

7   Piezoelectric materials can be grouped into three types, ceramic, polymer, and composite types (Ahmed

8   et al., 2017). Macro-Fiber Composite (MFC) with ceramic fibers is a composite material with excellent

9   electromechanical properties of ceramics as well as polymeric flexibility (Khazaee et al., 2019), that

10 makes it ideal material for long-endurance kinetic energy harvesting.

11 Unimorph geometry is one of the most widely used configuration for PEHs (Li et al., 2014), in which

12 one piezoelectric layer is bonded into a non-piezoelectric substrate shim with clamped-free boundary

13 condition. A number of researchers used MFC materials for PEH in unimorph configuration (Erturk et

14 al., 2008; Khazaee et al., 2019; Shan et al., 2015; Sodano et al., 2006). Shan et *al.* (Shan et al., 2015)

15 used a bonded beam from MFC and polyvinyl chloride layers in clamp-free boundary condition. The

16 beam was subjected to water vertexes induced from an upstream cylinder for PEH and obtained a

17 maximum output power of 1.32 µW. Moreover, by an experimental study, Sodano et *al.* (Sodano et al.,

18 2006) compared the maximum instantaneous power of three types of materials in unimorph geometry,

19 including the MFC material, over 12 bending modes and obtained 11.714 µW at third bending mode.

20 Obtaining maximum power from vibration sources is the main research subject within PEHs. Reddy et

21 al. (Reddy et al., 2016) introduced a cavity inside the substrate beam in order to enhance harvested power

22 from PEHs. In the context of power estimation, it is a well-known fact that damping has a critical role

23 on the output power by PEHs (Roundy et al., 2003). Four factors contribute into energy dissipation of

24 unimorph PEHs, namely energy dissipation from air resistance force, squeeze force, internal energy

25 dissipation and support loss (Hosaka et al., 1995).

26 Internal energy dissipation in composite structures is a parameter influenced by five factors, namely

27 matrix or fiber viscoelasticity, interphase, damage, viscoplastic, and thermoelastic (Bhattacharjee and

28 Nanda, 2018; Chandra et al., 1999). In almost all numerical and experimental studies on PEHs, a perfect

29 bonding have been assumed, while adhesion loss or debonding due to the aging or improper

1 manufacturing process is a major concern about adhesive joints (Pazand and Nobari, 2017). Saravanos

2 and Hopkins (Saravanos and Hopkins, 1996) showed that delamination cracks between layers of a

3 composite beam increases modal damping of the beam. Although debonding can have a substantial effect

4 on damping (Khazaee et al., 2018) and consequently will change the PEH power dramatically, yet there

5 is no investigation on effect of this damage on the output power.

6 Support loss, also called clamping loss, is the energy dissipated from a vibrating structure through its

7 support. As the structure undergoes flexural vibration, it excites its support both by shear and moment

8 forces causing elastic wave propagating into the support, which consequently leads to energy absorption

9 by the support (Hao et al., 2003). Chen et *al.* (Chen et al., 2017) looked at the support loss in micro-

10 electromechanical systems and introduced it as the inverse of quality factor, which can be obtained

11 through elastic wave propagation through the support. Although all the cantilever clamps are created by

12 screw joints, these studies (Chen et al., 2017; Hao et al., 2003) did not consider the effect of joint

13 characteristics on the support loss. If the joints are used to provide clamps, then friction regions due to

14 the bolted joints may cause slipping, which is a source of damping (Goyder, 2018). An important source

15 of energy dissipation in bolted joints is joint tightness. High clamping pressure produces greater

16 penetration forces (Ibrahim and Pettit, 2005). Since unimorph geometry is built by clamping piezoelectric

17 harvester with the screw, any source of energy dissipation in the clamps, including joint tightness, should

18 be considered for investigation of power generation by a piezoelectric.

19 Within energy harvesting research area, which is highly dependent on the different aspects of vibrational

20 characteristics of the device, there is lack of studies investigating the dependency of the power to

21 vibrational features within the system such as damage and support damping mechanisms. Thus, in this

22 paper a series of experimental studies are carried out to investigate the effect of debonding, as one of the

23 regular defect in adhesive layers, and support loss on output power of a composite beam with MFC

24 piezoelectric layer. In addition, using a single degree of freedom method, change of the power with

25 respect to debonding and support loss is modelled as the damping variation within the system.

26 2. A Modeling Technique for Unimorph Harvester

27 There are various techniques for modelling piezoelectric energy harvesters ranging from simple one

28 degree of freedom (1-D) to two-dimension multi degree of freedom methods. While 1-D methods require

1   less parameters to model the system, other methods require more parameters to be defined and are

2   computationally time consuming. On the other hand, as proposed by Erturk and Inman (Erturk and

3   Inman, 2008), a 1-D method that considers electro-mechanical coupling can be a suitable method for

4   assessment the behavior of a piezoelectric harvester. Moreover, 1-D methods were previously used for

5   studying piezoelectric energy harvesters by researchers (DuToit et al., 2005; DuToit and Wardle, 2007;

6   Roundy et al., 2003). As in this paper experimental data and analytical model will be correlated for

7   obtaining damping coefficient in many case studies, it is desirable to keep the model as simple as possible

8   and at the same time accurate. Hence, a 1-D model with electro-mechanical coupling will be handled

9   into a suitable form for our investigation by elaborating damping coefficient in this model. In the result

10   section, the accuracy of the model to predict experimental data will be presented. Figure 1 presents the

11   schematic of the model, which comprises a piezoelectric mass with internal resistance of R_p, and a proof

12   mass simply connected to a load resistor, R_l. This model is valid for the case that there is no substrate

13   shim. In order to comprise effect of the substrate, a coefficient, α_m, which is the proportion of

14   piezoelectric mass to device mass, is added. Therefore, the equations of motion for a piezoelectric

15   harvester with the substrate and piezoelectric layer can be shown as (DuToit et al., 2005):
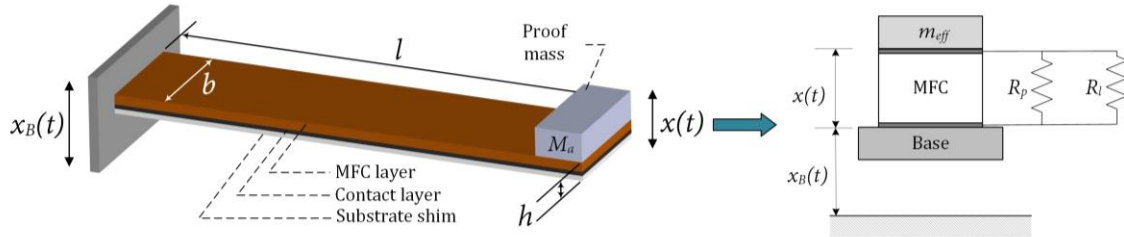
16

17   *Figure 1. Single degree of freedom electromechanical model* (DuToit et al., 2005)

$$\ddot{x}(t) + 2\,\zeta_m \omega_n \dot{x}(t) + \omega_n^2\, x(t) - \alpha_m \omega_n^2 d_{31} V_p(t) = -\ddot{x}_B(t) \qquad (1)$$

$$R_{eq} C_p \dot{V}_p(t) + V_p(t) + m_{eff} R_{eq} d_{31} \omega_n^2 \dot{x}(t) = 0 \qquad (2)$$

18   , where $\ddot{x}_B$ [m/s^2] is the base excitation acceleration, x [m] is the relative displacement of harvester tip

19   respect to the base, ω_n [1/rad] is the undamped natural frequency of harvester defined as $\sqrt{k/m_b}$, ζ_m is

20   the mechanical viscous damping ratio, V_p [V] is the output voltage and $m_{eff} = M_a + m_p/3$ [kg] (DuToit

21   et al., 2005) is the effective mass of piezoelectric layer contributed to shunt damping effect. The

1 overhead dot indicates the time derivative. In addition, d_{31} [C/N] is the piezoelectric coupling coefficient

2 in 3-1 mode, R_{eq} [Ω] is the equivalent electric resistance, C_p is the capacitance of the piezoelectric. The

3 capacitance is defined in terms of dielectric constant K, the permittivity of free space (ε₀=8.9 nF/m),

4 piezoelectric area A_p [m^2] and thickness t_p [m] with $C_p = K \, \varepsilon_0 A_p/t_p$.

5 If the base excitation is assumed to be harmonic, $\ddot{x}_B(t) = \bar{X}_B e^{j\omega t}$, then the displacement and voltage

6 will be a harmonic function with the same frequency but with different phase, e.g. $V_p(t) = \bar{V}_p e^{j\omega t + \varphi}$ and

7 $x(t) = \bar{X} e^{j\omega t + \varphi}$. By defining magnitude of power to be $\bar{P}_{out} = (\bar{V}_p)^2/R_{eq}$, it can be expressed as

8 (DuToit et al., 2005):

$$\left| \frac{\bar{P}_{out}}{\bar{X}_B} \right| = \frac{(1/\omega_n) m_{eff} \, r \, k_e^2 \left(R_{eq} / R_l \right)_{31} \Omega^2}{\sqrt{\left[\left(1 - \left(1 + 2r\zeta_m\right)\Omega^2\right)^2 + \left(\left(2\zeta_m\Omega\right) + \left(r\Omega - r\Omega^3\right) + \alpha_m r k_e^2\Omega\right)^2 \right]}}, \tag{3}$$

9 where $r = R_{eq}\omega_n C_p$ is dimensionless resistance term, $\Omega = \omega/\omega_n$ is dimensionless frequency, and k_e is

10 the electromechanical coupling factor defined with $k_e^2 = k_{31}^2/(1 - k_{31}^2)$. As it can be seen from Eq.(3),

11 apart from physical properties of piezoelectric harvester, output voltage depends on load resistance and

12 excitation frequency for a given excitation magnitude. Output power from piezoelectric is maximum at

13 an optimum load resistance called optimum load, R_{opt}. Moreover, if the maximum power at short-circuit

14 and open-circuit conditions is plotted against frequency, two frequencies are assigned to maximum power

15 that are called short-circuit, ω_{sc}, and open-circuit resonant frequencies, ω_{oc}, respectively. According to

16 these values, one can calculate the electromechanical coupling factor, k_e, of piezoelectric harvester with

17 $k_e^2 = \sqrt{(\omega_{oc}/\omega_{sc})^2 - 1}$.

18 The presented model is a simple 1-D model. However, because output power obtained by this method is

19 expressed in terms of coefficients that will be obtained experimentally, see Eq.(3), the model will present

20 accurate data compared to the experimental data, as was proved in (DuToit and Wardle, 2007). For

21 example, ω_n can be obtained through experimental tests and by evaluating ω_{oc} and ω_{sc} through

22 measurements of power over a wide frequency range, k_e will be accordingly calculated. The only

23 parameter that should be investigated is damping coefficient. The analytical model assigned a single

24 coefficient, e.g. ζ_m, for considering energy dissipation in the energy harvesting system in cantilever

1   configuration. On the other hand, in the presented study, it is aimed to capture the effects of two sources

2   of damping mechanisms, e.g. damage damping and support loss, which have different natures. Thus, to

3   make the damping model closer to the actual one, all sources of energy dissipation in the system will be

4   identified and then all the other damping mechanisms apart are evaluated analytically while damage and

5   support loss damping will be extracted according to the measurements.

6   Energy dissipation consists of internal energy dissipation, fluid-structural viscous damping and support

7   loss due to the cantilever boundary condition and for the case of deboned sample, a damaged damping

8   term should be considered. These sources of energy dissipation are shown in Figure 2. So, ζ_m can be

9   expressed with Eq. (4).

$$\zeta_m = \zeta_{Structural} + \zeta_{Fluid-Structure} + \zeta_{Support} + \zeta_{Damage} \tag{4}$$

10   Fluid-structural damping, $\zeta_{Fluid-Structure}$, is considered to be due to airflow force due to vibration of beam

11   in free air and squeeze force due to airstream force from the near fixed boundary wall. Internal energy

12   dissipation, $\zeta_{Structural}$, is the energy dissipated inside material, which is an energy dissipation source inside

13   the beam. Fluid-structural damping terms are more straightforward to deal with and some analytical

14   formula were reported for them, such as (Hosaka et al., 1995), as it is less difficult to estimate the

15   resistance force against beam transverse vibration induced from surrounded fluid. On the other hand,

16   damage (ζ_{Damage}) and support loss ($\zeta_{Support}$) mechanisms are difficult to deal with and are often measured

17   according to experimental data. In this research, fluid-structural and internal energy dissipation

18   mechanisms are calculated according to analytical expressions see Eq. (5) (Hosaka et al., 1995), and the

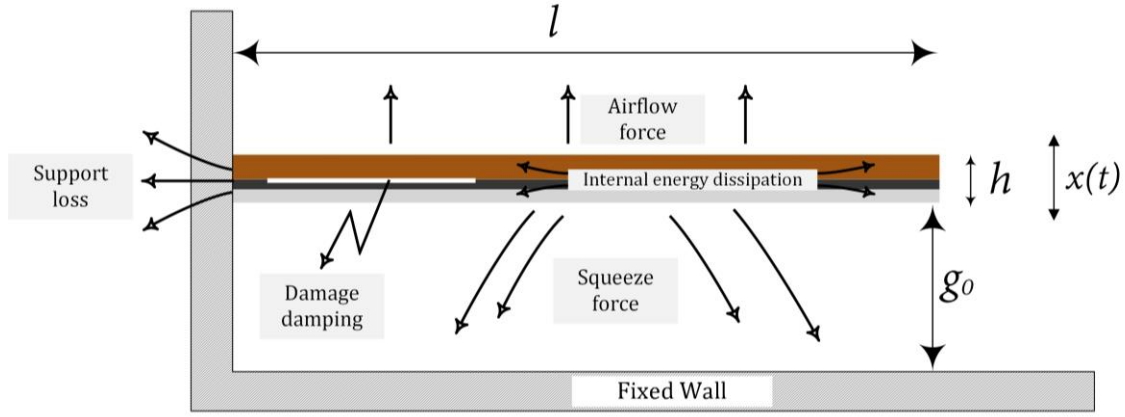19   support loss and damage damping mechanisms are evaluated based on experimental data.

Figure 2. Different sources of energy dissipation considered in this study

$$\zeta_{Fluid-Structure} = \frac{\mu b^2}{2\rho_b g_0^3 h \omega_n} + \frac{\frac{3}{4}\pi b^2 \sqrt{2\rho_{air}\mu\omega_n}}{2\rho_b hbl \omega_n}$$

(5)

$$\zeta_{Structural} = \eta/2$$

where μ and ρ_{air} are dynamic viscosity and density of air. In addition, g_0 is the distance between the fixed wall and beam outer surface as shown in Figure 2 and η is the structural damping coefficient and in this study a value of 0.5×10^{-6} is considered (Blom et al., 1992).

Due to the presence of damping in the equation for output power, Eq. (3), damping will have a significant effect on the output power in a unimorph energy harvester. This work aims to investigate the effect of changing the damping coefficient, ζ_m, through debonding and the support tightness, on the output power while four damping mechanisms are considered in the presented study, see Eq. (4). Hence, it is necessary to capture the actual variation of the energy dissipation source under study. In section 4, support loss damping will be evaluated from the defect-free state, which this value will be used for the deboned state and hence the actual damage damping due to debonding will be evaluated. In section 5, there is no damage damping and support damping can be directly evaluated from experimental data.

3. Experimental Procedure

The effects of the debonding and support loss on the output power were investigated through experiments. The experiments were carried out with piezoelectric samples in unimorph geometry. The

1   piezoelectric samples were clamped with a clamp box on one end. Then, it is excited with a magnetic

2   vibration shaker by sinusoidal input signal, where its response in terms of output voltage and current

3   were recorded. Figure 3 shows the configuration of the piezoelectric energy harvesters throughout the

4   study.

5   The piezoelectric layer is a MFC with elastic modulus of 30.336 GPa and 15.857 GPa in x- and y-

6   directions, respectively, and Poisson's ratios of 0.31 in xy and 0.16 in yx and shear modulus of 5.515

7   GPa. Thickness of the MFC is 0.30 mm while the thickness of the PZT fibers are 190 µm with density

8   of active area of 5.44 g/cm^3. The electromechanical properties of the piezoelectric layer are d_{33}= 460

9   pC/N, and d_{31}= -210 pC/N. The center shim is made of aluminum with thickness of 0.12 mm, elastic

10   modulus of 68.9 GPa and density of 2.7 g/cm^3. The piezoelectric layer is bonded to the center shim with

11   epoxy rapid 332 adhesive with density of 1.16 g/cm^3. In the case of investigating debonding effects in

12   section 4, thickness of bond layer in perfect and poorly cured bond conditions are 400 and 189 µm,

13   respectively. In section 5, where the effect of support loss damping is investigated, the bond layer

14   thickness equals to 245 µm.
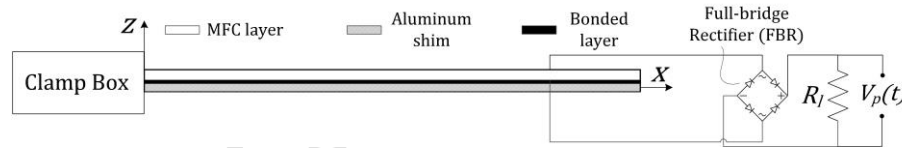
15

16   *Figure 3. Piezoelectric energy harvester configuration*

17   The aforementioned unimorph energy harvester is excited with a VSD 201 Shaker while its input voltage

18   and electrical power are measured. Signal generation and data recording were carried out with National

19   Instrument modules. For signal generation, NI 9263 module, a 4-channel ±10 V 16-Bit Analog Voltage

20   Output, which is adjusted by LabVIEW^{TM} 2013 is connected to a Kepco AC power generation and the

21   output from Kepco power supply is wired to the shaker. A NI 9215 module with 4-channel ±10 V 16-Bit

22   Analog Voltage Input is used for recording voltage output of the piezoelectric harvester. A National

23   Instrument Compact data acquisition system (cDAQ) type 9172 is used as the medium between the

1 modules and experimental components, e.g. the shaker and piezoelectric samples. Figure 4 shows the

2 experimental setup.

3

4
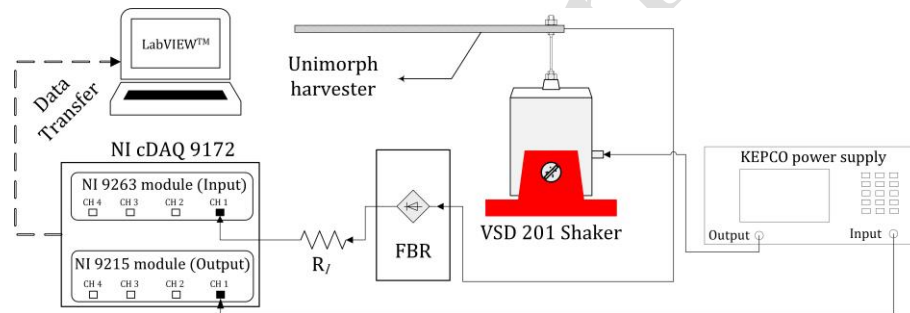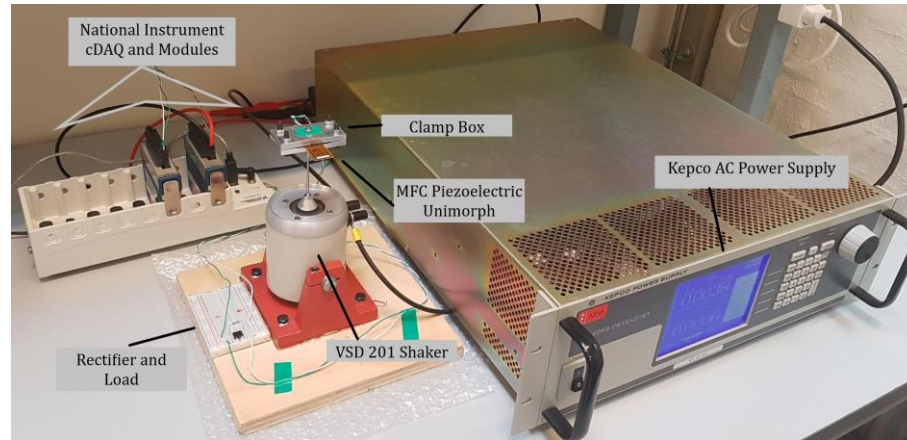
5 *Figure 4. Setup for measuring voltage output*

6 **4. Debonding Effects**

7 During the model derivation for the piezoelectric energy harvester from vibration, mostly cantilever

8 configuration is considered with the perfect bonding between piezoelectric and metal substrate. In

9 practice, the perfect bonding assumption may be degraded over time during operation or during

10 manufacturing process in the first stage (Pazand and Nobari, 2017). In particular, as the loading condition

11 is dynamic and the harvester mostly vibrates close to its fundamental natural frequency, it is likely to

12 observe debonding between the substrate and the piezoelectric layer. The debonding might have two

13 influences on the output power. An obvious effect is that, it prevents the vibration of a part of the energy

14 harvester, so it will reduce the active area for power generation. Moreover, the debonding may increase

15 the damping ratio of the device, which results to less power generation. This increment in the damping

1   depend on the vibration mode (Khazaee et al., 2018). In this section, an experimental verification of the

2   debonding effect on the output power is presented.

3   Two samples are tested with the same length and width, each consisting of a 0.3 mm thickness MFC

4   piezoelectric layer. The samples are bonded to an aluminum substrate with 0.12 mm thickness by epoxy

5   rapid 332 adhesive. The thickness of bond layers are 400 and 189 µm in pristine and poorly cured bond

6   samples, respectively. Figure 5 shows the pristine and debonded samples with capacitance of C_p=177.07

7   nF/m for an active length of 85 mm. The piezoelectric harvester is connected to a 31500-Ω resistance

8   load. The unimorph is excited over frequency range of 5 to 100 Hz with 1 Hz frequency step with the

9   same excitation amplitude. Three replications are used to show the repeatability of tests.
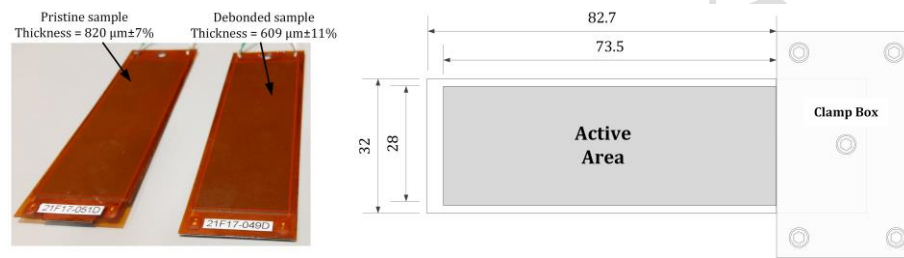
10

11   *Figure 5. MFC pristine and debonded dimensions and unimorph configuration with clamp box*

12   *screws*

13   As can be interpreted from Figure 5, thickness of the adhesive layer for one sample was considered 211

14   µm less than the other sample to make it vulnerable to debonding due to inappropriate debonding

15   thickness. Then, the sample was excited by the shaker on its natural frequency until a debonding area is

16   initiated and developed. It is worth mentioning that after initiation of the debonding, the propagation was

17   quick. The samples were scanned using Acoustic Microscope KSI V8 from the aluminum substrate and

18   from MFC layer down to the other front side to find out the layers within them debonding is occurred.

19   Figure 6 shows the Acoustic Microscope KSI V8 for scanning the samples from the aluminum side.
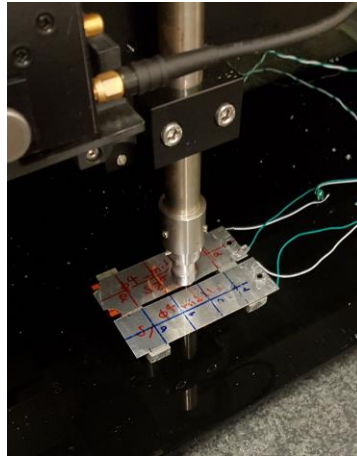
1

2   *Figure 6. Pristine and debonded samples scanned with Acoustic Microscope KSI V8*

3   Figure 7 shows the scanned pictures of the samples in depth with ultrasonic waves. Areas with different

4   colors in Figure 7 represent the regions with different densities. In order to recognize debonding regions,

5   similar regions with different colors should be observed at different depth levels. It has been observed

6   that, the debonding was initiated between aluminum shim and adhesive layer, as the color scattering in

7   the surface can be seen from Figure 7 (b) through (c). Since the dark color regions exist at different

8   depths, from Figure 7 (a)-(e), this area is the likelihood-debonding region. This region is marked with

9   white box in Figure 6. In addition, there are two regions with distinctive colors on the Figure 7 (e)-(f) on

10   the pristine sample, which based on thickness measurements is found to be the result of higher density

11   of adhesive in these regions.

(a)

(b)

(c)

(d)

(e)

(f)
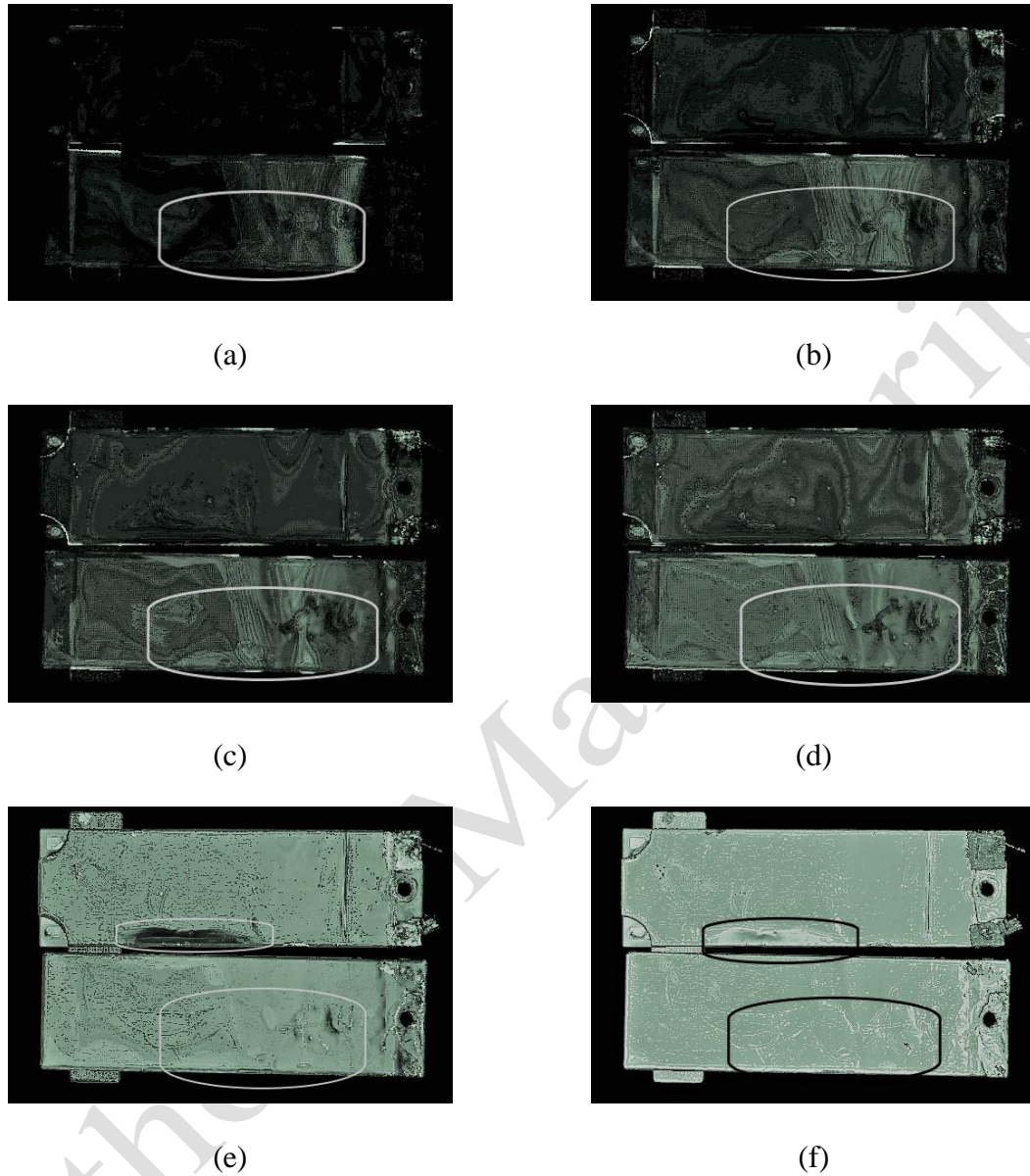
1   *Figure 7. Pristine (Top sample) and debonded (Bottom sample) samples scanned with ultrasonic*
2   *waves through depth from the aluminum shim side (a) to (f).*

3   Figure 8 shows the frequency spectrum of RMS of the power generation for three replications. Firstly,

4   the results obtained from the duplications are identical showing that the experiments are repeatable. As

5   it can be seen from the frequency spectrum, there are two peaks for the output power at frequencies of

6   30 Hz and 49 Hz. The first peak frequency is related to the device fundamental bending natural frequency,

7   while the second peak is result of anti-resonance frequency of the device. Anti-resonance frequency is

1   the result of electromechanical coupling. At this frequency, the voltage and current are considerably

2   different from resonance frequency even though the power is similar (DuToit et al., 2005).
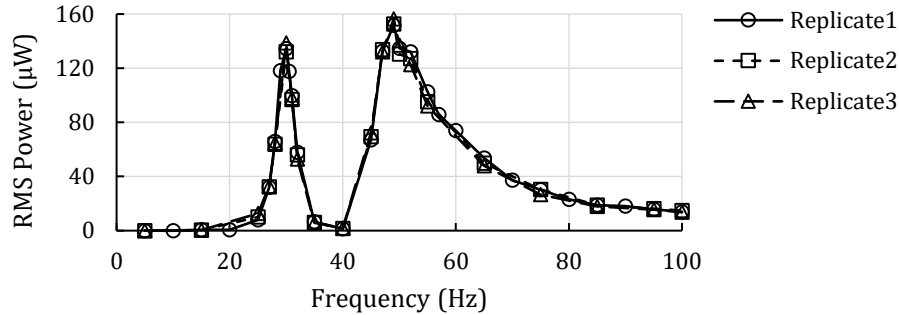
3

4   *Figure 8. Frequency spectrum of power for three replications on MFC sample*

5   The debonding reduces the active area in the device, which is an important factor in the power generation,

6   and it increases the internal structural. Figure 9 shows the output power from the pristine and debonded

7   samples as a function of frequency. Table 1 shows the variation of peak frequencies and output power

8   between pristine and debonded samples. The debonding reduces the device stiffness and, hence,

9   decreases the resonance and anti-resonance frequencies by 23 % and 18 %, respectively. Reductions in

10   the peak frequencies are in the same order showing the stiffness reduction of the beam. Moreover, the

11   presence of the debonding area causes a dramatic reduction in the output power at resonance and anti-

12   resonance frequencies. There are two reasons for reduction of the power generation due to the debonding,

13   reduction of the active area and increment in the damage damping. To measure the real debonding area,

14   the debonded sample is exploited and the debonding region is marked, as shown in Figure 10. The

15   debonding area is measured to be 15% of the active area. If a uniform generation of power assigned to

16   the whole area, 15 % active area reduction will reduce output power by 15 %. Hence, the rest of the

17   power reduction is due to increment of the damage damping. In addition, it can be noted from Figure 9

18   that, degradation of the output power is two times at the anti-resonance compared to at the power

1 reduction at the resonance frequency, proving that the power at anti-resonance is much more sensitive to

2 the debonding effect.
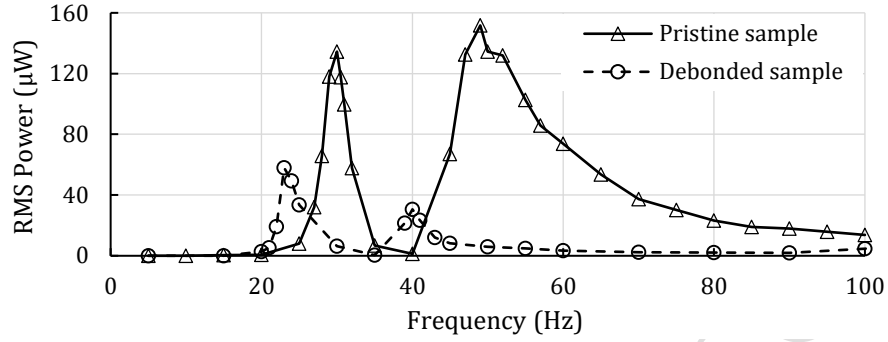
3

4 *Figure 9. Comparison between power for pristine and debonded samples over different frequencies*

5 *Table 1. Comparison between pristine and debonded samples*

Parameter	Pristine	Debonded	Variation (%)
Resonance frequency (Hz)	30	23	-23.3
Anti-resonance frequency (Hz)	49	40	-18.4
RMS of power at resonance	132.0	77.9	-41.0
RMS of power at anti-resonance	152.7	30.5	-80.0
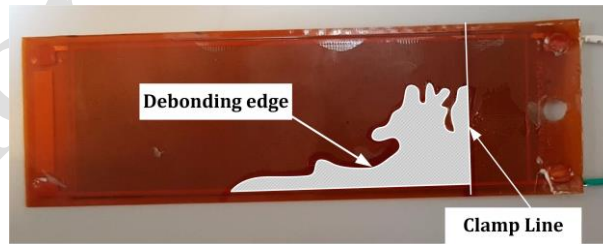
6

7 *Figure 10. Debonded area within adhesive and aluminum layer*

8 By applying the model presented by Eq. (3) and by updating the ζ_m through an error-minimization

9 process, the analytical output power is correlated with respect to the experimental output power. This

10 process is then repeated for the case that the debonding occurs by reduction of the active area. Figure 11

11 shows the comparison of the resonance power between the undamaged and bonded states based on the

12 analytical and experimental results, and variation of the mechanical damping obtained after the model

1 updating process. Figure 11 (a) shows that the power is successfully correlated at resonant by updating

2 damping in the presented model. The presented model with correlation factor has better accuracy at

3 resonant frequency compared to the other frequencies. However, as maximum available power is of

4 interest in energy harvesting applications and this maximum power is obtained at resonant, the presented

5 model can be used for maximum power correlation. Moreover, it can be seen from Figure 11 (a) that

6 correlation for pristine sample is more accurate than for the debonded sample. This is due to the

7 nonlinearity that is introduced into system due to debonding. As shown in Figure 11 (b), correlated

8 mechanical damping for the debonding sample shows that, the debonding caused to increase the ζ_m from

9 0.0483 to 0.0765. ζ_m comprises support loss, fluid-structural and internal friction damping mechanisms

10 for defect-free state and damage damping for the case of deboned state. Fluid-structural damping are the

11 same for both cases and will be evaluated using Eq. (5). Since during the tests boundary conditions

12 remained unchanged, support loss are identical for both pristine and deboned states. However, since

13 thickness of samples are slightly different for pristine and deboned samples, viscous damping coefficient

14 was calculated for each condition. Damage damping was calculated by subtracting the calculated

15 analytical fluid-structural, structural damping, experimentally obtained support loss damping from the

16 correlated mechanical damping.

(a)   (b)
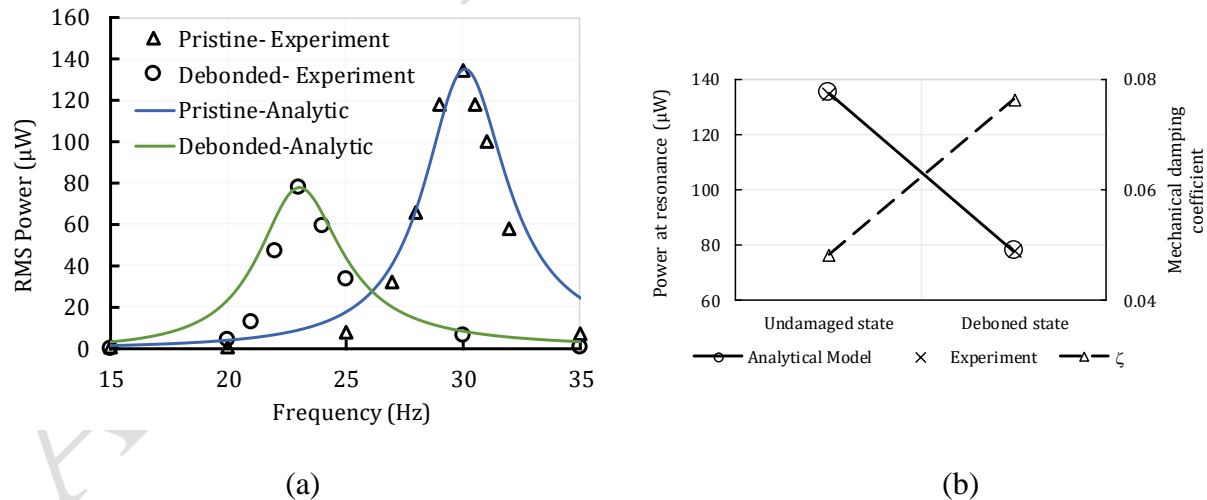
17 *Figure 11. (a) Correlated data versus experimental data and (b) comparison between maximum*

18 *power at resonance and damping increase due to debonding*

1   Table 2 summarizes the obtained results from this section. As it was shown previously, debonding area

2   reduces 15% of the active area that is responsible for power generation. However, this 15% debonding

3   area reduced the RMS resonant power density 20.53% from 60.83 to 48.34 $\mu W/cm^3$. Support loss, which

4   is obtained by subtracting fluid-structure and structural damping from correlated damping coefficient,

5   has a great contribution in the total damping proving that support loss damping is an important part of

6   energy dissipation in the system and hence the next section is dedicated to this support loss. Damage

7   damping in debonded sample is responsible for 27% of the total damping mechanisms showing that

8   debonding can greatly affect damping coefficient.

9   *Table 2. Variation of output power, mechanical damping and structural damping due to improper*

10   *bonding*

Parameter	Undamaged sample	Debonded sample
Active area (cm^2)	20.58	17.49
RMS resonant power density ($\mu W/cm^3$)	60.83	48.34
ζ_m (Correlated value)	4.83E-02	7.65E-02
$\zeta_{Fluid-Structure}$ (Eq. (5))	7.90E-04	1.24E-03
$\zeta_{Structural}$ (Eq. (5))	5.00E-07	5.00E-07
$\zeta_{Support}$ ($=\zeta_m- \zeta_{Fluid-Structure}- \zeta_{Structural}$)	4.75E-02	4.75E-02
ζ_{Damage} ($=\zeta_m- \zeta_{Fluid-Structure}- \zeta_{Structural}- \zeta_{Support}$)	-	2.78E-02

11   Nature of the damping variation due to delamination in the composite materials has been investigated by

12   Khazaee et al. (Khazaee et al., 2018). The variation in damping depends on the vibrating mode, which

13   causes penetration motion or slip motion between layers near the delamination (Khazaee et al., 2018).

14   Fundamental mode shape of the unimorph harvester is shown in Figure 12. In this mode, if a debonding

1 region is present, layers on top and bottom of the debonding area have a penetration motion in

2 perpendicular direction causing an extra energy dissipation mechanism inside the harvesting material.
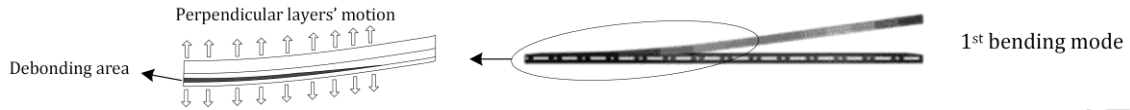
3

4 *Figure 12. Mechanical damping increases due to debonding in the first bending mode*

5. Support Loss Damping

6 Unimorph or bimorph is among the most applicable configuration of piezoelectric energy harvesters,

7 where one end is clamped and the other end is free. To create the clamp, often a part of the energy

8 harvester is clamped within a clamp box in which screws are tighten to provide non-moving area. Due

9 to this clamp, an extra loss is introduced into the system, called support loss (Hosaka et al., 1995). In this

10 section, output powers from a unimorph piezoelectric energy harvester under clamp-free boundary

11 condition with different clamp box configuration are compared to each other in order to study the effect

12 of the clamp characteristics on the output power.

13 Figure 12 (a) shows the sample for testing the support loss effect on the output power. The thickness of

14 MFC piezoelectric, adhesive and substrate layers are 300, 245 and 120 µm, respectively. The clamp box

15 consists of two 60×30 mm blocks with four screws placed symmetrically in the corners with 6 mm center-

16 to-edge distance and one center hole for the shaker attachment. To observe the effect of the support loss,

17 two types of materials were used for clamp box made by plastic and aluminum, as shown in Figure 13.

18 The weight of clamp box set with screws for aluminum and plastic types are 59.09 g and 25.86 g,

19 respectively. Moreover, the screws of clamp box were tighten with different torques and for each set of

20 torque; the power was measured over a frequency range close to its natural frequency.
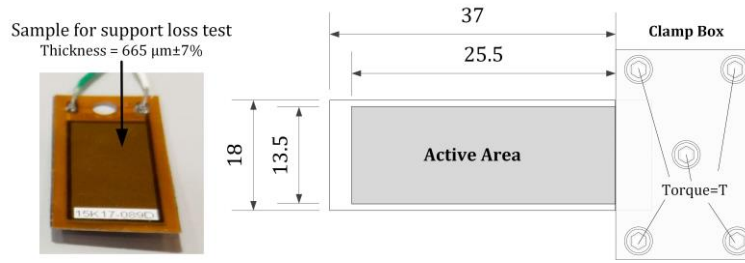
(a)
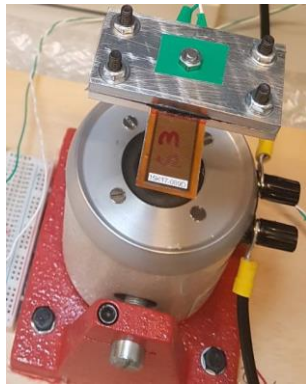
(b)

(c)

1 *Figure 13. (a) MFC harvester dimensions and unimorph configuration with clamp box screws, (b)*
2 *Aluminum and (c) plastic clamp boxes clamping the MFC harvester*

3 Figure 14 shows the output power density in µW/g over a frequency range including the resonant

4 frequency of piezoelectric energy harvester, where g= 9.81 m/s^2, from the MFC sample with the

5 aluminum and plastic clamp boxes at different levels of tightening torques. The vertical axis shows the

6 output power normalized to input base acceleration in terms of root mean square (RMS), when MFC

7 sample were excited by a harmonic excitation with the maximum force of 17.8 N. For each case of

8 excitation with the specific frequency, output voltage and current were measured with 31500-Ω

9 resistance load and then power was calculated by product of voltage and current. Tightening torque,

10 measured in N.m. unit, was the torque used for fastening the four screws of clamp box as well as the

11 shaker attachment screw as shown in Figure 12 (a) and measured with the torque meter used for applying

12 the torque. A sample of measured voltage, current and output power for plastic clamp box with tightening

1   torque 0.5 N.m and excitation frequency of 220 Hz are shown in Figure 15. The immediate conclusion

2   of Figure 14 is that, output power spectrums represent different values for different clamp box materials

3   and tightening torques proving that clamping characteristics play an important role in energy harvesting

4   from cantilevered piezoelectric beams. The resonant frequency, as displayed in Figure 16, for plastic

5   clamp lies in the interval [212.1,220.4] Hz with an average of 215.8 Hz is higher than resonant frequency

6   for aluminum clamp with an average of 199.5 Hz lying in the interval [198.4,202.1] H. Moreover, it can

7   be seen that the tightening torque on the clamp box will change the output power of the energy harvester

8   as well as slightly alters the resonant frequency of piezoelectric harvester. Output RMS power at

9   resonance equals to 0.39 for T=0.5 N.m while this figure is 0.26 µW/g for T=0.8 N.m, when aluminum

10 clamp box is used, showing a 33% reduction in output power due to tightening torque. This power

11 reduction for plastic clamp box is 14% showing a lower dependency of power to tightening torque

12 compared to aluminum clamp box. In addition, resonant frequency varies maximum 3.7% in the case of

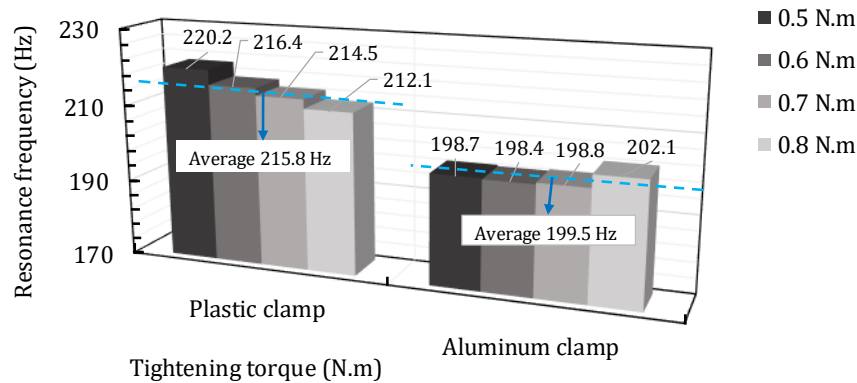13 plastic clamp while this variation equals to maximum 1.7% for aluminum clamp.
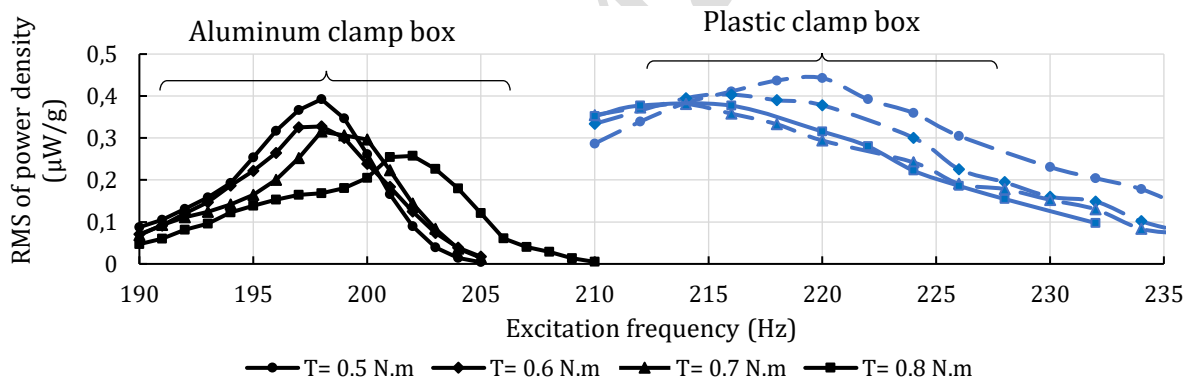
14

15 *Figure 14. Power frequency spectrum for sample 3 over changing torque T of aluminum clamp boxes*
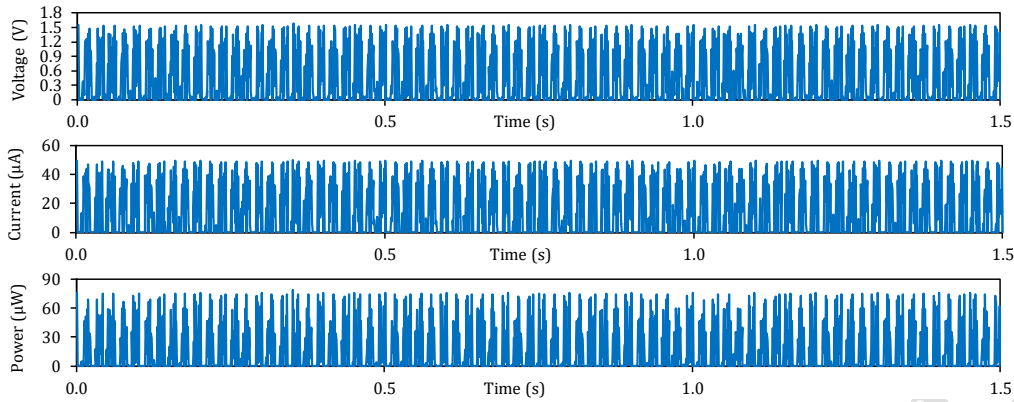
Figure 15. Voltage, current and power from piezoelectric harvester with plastic clamp with T=0.5 N.m at 220 Hz excitation

Figure 16. Resonant frequency of piezoelectric harvester for different tightening torques on plastic and aluminum clamps

Output current signals over a 1.5-second period from piezoelectric harvester with plastic clamp vibrating at its resonant frequency for different tightening torques are displayed in Figure 17. The RMS of output currents for tightening torques of 0.5, 0.6, 0.7 and 0.8 N.m are 23.8, 22.2, 21.9 and 21.7 µA showing that increasing tightening torque on cantilever clamp box reduces output current. Increasing tightening torque from 0.5 to 0.6 N.m reduced current by 6.7% while this drop is 1.4% for 0.6 to 0.7 N.m and 0.9% for 0.7 to 0.8 N.m tightening torque. Figure 18 shows the power at the resonance at different levels of tightening torque for the aluminum and plastic clamp boxes. Since the plastic clips have a degree of flexibility, to prove that the trend is reciprocal, the tests were performed from the lowest torque, T= 0.5 N.m, to the

highest torque, T=0.8 N.m and vice versa. The results show that, the harvester with the aluminum clamp box produced lower power. On the other hand, by increasing the tightening torque of the screws of the clamp box, RMS of the maximum power decreases, for the both aluminum and plastic clamps. Figure 18 implies that, the plastic clips, which are more flexible than the aluminum, can provide higher output power and lower support loss compared to that one with the aluminum clamp.
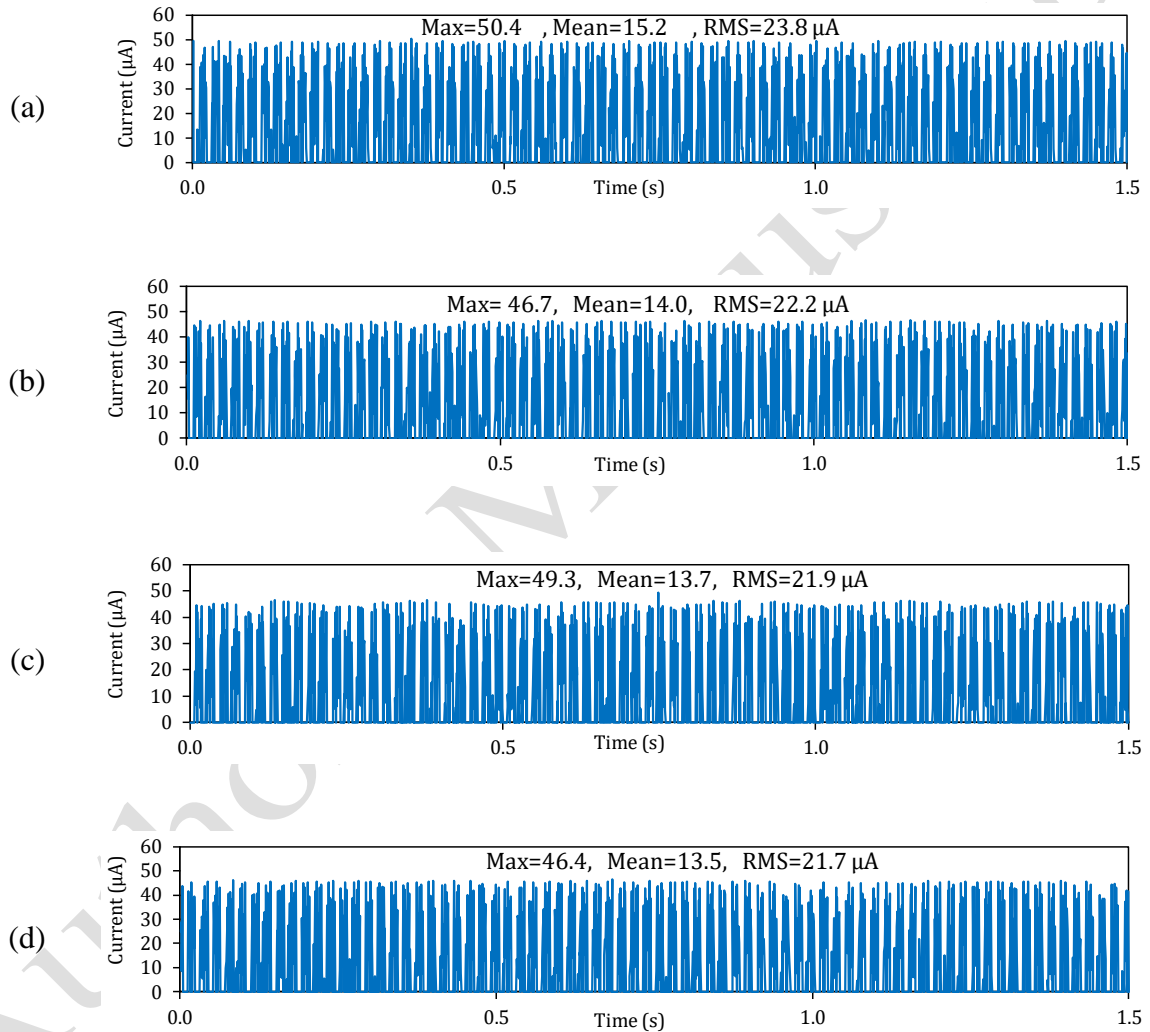
Figure 17. Comparison between current measurements at resonant frequency excitation for plastic clamp at tightening torque (a) 0.5 N.m, (b) 0.6 N.m, (c) 0.7 N.m and 0.8 N.m
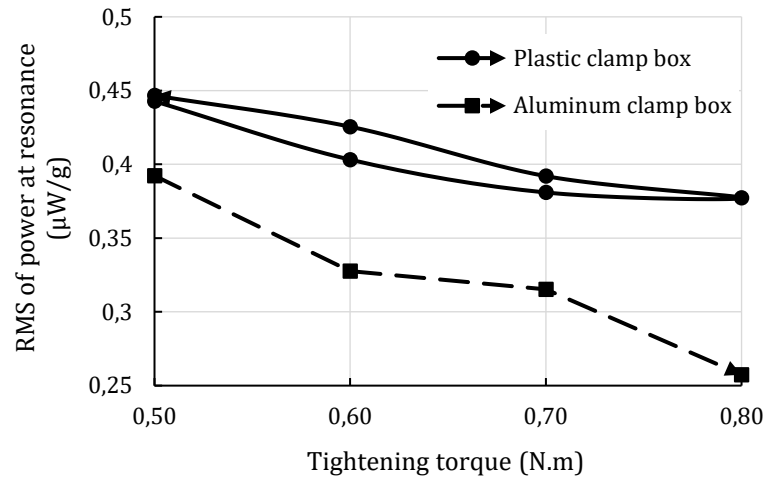
Figure 18. Variation of power versus torque applied on clamp screws for different clamp box

Similar to the previous section, using the developed model for the unimorph harvester, and with the minimization of the error between the maximum resonance powers, the mechanical damping ratios are identified for different clamp boxes at different tightening levels. These identified damping ratios are shown in Figure 19. Overall, aluminum clamp introduces higher energy dissipation, which in turn causes to reduce the damped natural frequency in Figure 14. Therefore, in comparison with the aluminum clamp box with higher support damping, the lower resonance frequency of the harvester with the plastic clamp box is due to lower support damping. However, with increasing the clamp pressure by higher tightening torque, the support loss increases for both clamp boxes, independent to clamp material.
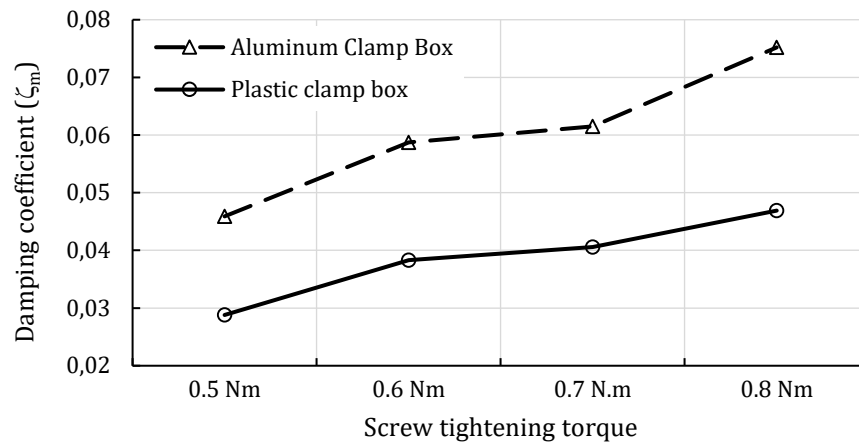
Figure 19. Variations of identified damping variations versus clamp pressure for aluminum and plastic clamps

6. Conclusions

This study presented an experimental investigation of effect of damage and support losses damping mechanisms on the output power of piezoelectric energy harvesters in unimorph geometry. The results show that, using a simple, but practical, single degree of freedom model, the power variation can be modelled with the mechanical damping variation. The debonding, as an internal source of damping inside the harvester, is investigated in this study. It is concluded that, the debonding increases the damping and reduces the output power dramatically. Moreover, the support loss, as an external damping source, has an effect on the output power in such a way that the clamp material as well as clamp pressure will change the output power.

Declaration of Conflicting Interests

The author(s) declared no potential conflicts of interest with respect to the research, authorship, and/or publication of this article.

References

Ahmed R, Mir F and Banerjee S (2017) A review on energy harvesting approaches for renewable

energies from ambient vibrations and acoustic waves using piezoelectricity. *Smart Materials and Structures* 26(8). IOP Publishing: 085031. DOI: 10.1088/1361-665X/aa7bfb.

Bhattacharjee A and Nanda BK (2018) Damping study of composites using wavelet analysis. *JVC/Journal of Vibration and Control* 24(21): 5141–5151. DOI: 10.1177/1077546317745256.

Blom FR, Bouwstra S, Elwenspoek M, et al. (1992) Dependence of the quality factor of micromachined silicon beam resonators on pressure and geometry. *Journal of Vacuum Science & Technology B: Microelectronics and Nanometer Structures* 10(1): 19–26. DOI: 10.1116/1.586300.

Chandra R, Singh S p. and Gupta K (1999) Damping studies in fiber reinforced composites- a review. *Composite Structures* 46(1): 41–51.

Chen SY, Liu JZ and Guo FL (2017) Evaluation of support loss in micro-beam resonators: A revisit. *Journal of Sound and Vibration* 411. Elsevier Ltd: 148–164. DOI: 10.1016/j.jsv.2017.08.048.

DuToit NE and Wardle BL (2007) Experimental Verification of Models for Microfabricated Piezoelectric Vibration Energy Harvesters. *AIAA Journal* 45(5): 1126–1137. DOI: 10.2514/1.25047.

DuToit NE, Wardle BL and Kim SG (2005) Design considerations for MEMS-scale piezoelectric mechanical vibration energy harvesters. *Integrated Ferroelectrics* 71: 121–160. DOI: 10.1080/10584580590964574.

Erturk a, Bilgen O, Fontenille M, et al. (2008) Piezoelectric energy harvesting from macro-fiber composites with an application to morphing wing aircrafts. *Proceedings of the 19th International Conference of Adaptive Structures and Technologies*.

Erturk A and Inman DJ (2008) Issues in mathematical modeling of piezoelectric energy harvesters. *Smart Materials and Structures* 17(6). DOI: 10.1088/0964-1726/17/6/065016.

Goyder HGD (2018) Damping Due to Joints in Built-Up Structures. In: Brake MRW (ed.) *The Mechanics of Jointed Structures: Recent Research and Open Challenges for Developing Predictive Models for Structural Dynamics*. Cham: Springer International Publishing, pp. 135–147. DOI: 10.1007/978-3-319-56818-8_11.

Hao Z, Erbil A and Ayazi F (2003) An analytical model for support loss in micromachined beam

1   resonators with in-plane flexural vibrations. *Sensors and Actuators, A: Physical* 109(1–2): 156–164.
2   DOI: 10.1016/j.sna.2003.09.037.

3   Hosaka H, Itao K and Kuroda S (1995) Damping characteristics of beam-shaped micro-oscillators.
4   *'Sensors and Actuators, A: Physical'*. DOI: 10.1016/0924-4247(95)01003-J.

5   Https://www.piezotech.eu (n.d.) PiezeTech Arkema Group.

6   Ibrahim RA and Pettit CL (2005) Uncertainties and dynamic problems of bolted joints and other
7   fasteners. *Journal of Sound and Vibration* 279(3–5): 857–936. DOI: 10.1016/j.jsv.2003.11.064.

8   Khaligh A, Zeng P and Zheng C (2010) Kinetic Energy Harvesting Using Piezoelectric and
9   Electromagnetic Technologies; State of the Art. *Industrial Electronics, IEEE Transactions on* 57(3):
10   850–860. DOI: 10.1109/TIE.2009.2024652.

11   Khazaee M, Nobari AS and Aliabadi MHF (2018) *Experimental Investigation of Delamination Effects*
12   *on Modal Damping of a CFRP Laminate, Using a Statistical Rationalization Approach.*
13   *Computational and Experimental Methods in Structures.* DOI: 10.1142/9781786344977_0003.

14   Khazaee M, Rezaniakolaei A and Rosendahl L (2019) An experimental study on macro Piezoceramic
15   fiber composites for energy harvesting. *Materials Science Forum* 951: 3–8. DOI:
16   https://doi.org/10.4028/www.scientific.net/MSF.951.3.

17   Li H, Tian C and Deng ZD (2014) Energy harvesting from low frequency applications using piezoelectric
18   materials. *Applied Physics Reviews* 1(4): 0–20. DOI: 10.1063/1.4900845.

19   Mortazavinatanzi S, Rezaniakolaei A and Rosendahl L (2018) Printing and folding: A solution for high-
20   throughput processing of organic thin-film thermoelectric devices. *Sensors (Switzerland)* 18(4):
21   989. DOI: 10.3390/s18040989.

22   Pazand K and Nobari AS (2017) Investigation of damage effect on the effective dynamic mechanical
23   properties of an adhesive in linear and nonlinear response regimes. *Journal of Vibration and Control*
24   23(14). DOI: 10.1177/1077546315612904.

25   Qing S, Rezania A, Rosendahl LA, et al. (2018) Characteristics and parametric analysis of a novel
26   flexible ink-based thermoelectric generator for human body sensor. *Energy Conversion and*

1   *Management* 156: 655–665. DOI: 10.1016/j.enconman.2017.11.065.

2   Reddy AR, Umapathy M, Ezhilarasi D, et al. (2016) Improved energy harvesting from vibration by
3   introducing cavity in a cantilever beam. *JVC/Journal of Vibration and Control* 22(13): 3057–3066.
4   DOI: 10.1177/1077546314558498.

5   Roundy S, Wright PK and Rabaey J (2003) A study of low level vibrations as a power source for wireless
6   sensor nodes. *Computer Communications* 26(11): 1131–1144. DOI: 10.1016/S0140-
7   3664(02)00248-7.

8   Saravanos D a. and Hopkins D a. (1996) Effect of delamination on the damped dynamic characteristics
9   of composite laminates. analysis and experiments. *Journal of Sound and Vibration* 192(2): 977–
10   993. DOI: 10.1006/jsvi.1996.0229.

11   Shan X, Song R, Liu B, et al. (2015) Novel energy harvesting: A macro fiber composite piezoelectric
12   energy harvester in the water vortex. *Ceramics International* 41(S1). Elsevier: S763–S767. DOI:
13   10.1016/j.ceramint.2015.03.219.

14   Sodano HA, Lloyd J and Inman DJ (2006) An experimental comparison between several active
15   composite actuators for power generation. *Smart Materials and Structures* 15(5): 1211–1216. DOI:
16   10.1088/0964-1726/15/5/007.

17